

Kinematics of the November 12, 1999 (Mw=7.2) Düzce Earthquake Deduced from SAR Interferometry

ZİYADİN ÇAKIR¹, AYKUT A. BARKA², JEAN-BERNARD DE CHABALIER³,
ROLANDO ARMIJO³ & BERTRAND MEYER³

¹ İstanbul Technical University, Faculty of Mines, Geological Engineering Department, Ayazağa,
TR-80626 İstanbul, Turkey (e-mail: cakirz@itu.edu.tr)

² Deceased; formerly of İstanbul Technical University, Institute of Eurasian Earth Sciences, Ayazağa,
TR-80626 İstanbul, Turkey

³ Institut de Physique du Globe de Paris (UMR 7578 CNRS), 4 Place Jussieu, 75252 Paris Cedex 05, France

Abstract: On November 12 1999, a destructive earthquake struck the Düzce area, following the 17 August 1999 İzmit earthquake that had occurred to the west about 3 months earlier. The Mw=7.2 Düzce earthquake was somewhat interesting in several ways. The most surprising feature of this earthquake is related to its rupture geometry, which appears to contradict what is commonly observed in strike-slip earthquakes. First, compared to its magnitude, the length of the surface rupture mapped in the field was rather short (~35 km). Second, according to seismic and some geodetic observations, the fault plane dips to the north at a very low angle ranging from 53° to 73° despite its predominant strike-slip motion, which is also inconsistent with tectonic field observations. In this study, the coseismic surface deformation caused by the November 12 1999 Düzce earthquake is mapped using Synthetic Aperture Radar interferometry (InSAR), and to constrain the rupture geometry, the InSAR data is modelled together with the coseismic GPS measurements using an elastic dislocation method. Modelling the geodetic observations with a linear inversion technique shows that the Düzce earthquake might have been associated with multiple fault breaks involving a near-vertical Düzce Fault and a reactivated old thrust fault that dips to the north.

Key Words: Düzce earthquake, SAR Interferometry, GPS, elastic modelling, source parameters

12 Kasım 1999 Düzce Depremi Kinematığının SAR Interferometrisi Yöntemiyle Ortaya Çıkartılması

Özet: 17 Ağustos 1999 İzmit depreminden yaklaşık üç ay sonra Düzce bölgesi 12 Kasım 1999 tarihinde yeniden yıkıcı bir depremle sarsıldı. Mw=7.2 Düzce depremi bazı yönleri ile ilginç bir depremdir. En şaşırtıcı özelliği kırık geometrisi ile ilgilidir. İlk olarak, depremin büyüklüğü ile kıyaslandığında arazide haritalanan deprem yüzey kırığı oldukça kısadır. İkinci olarak, sismolojik ve bazı jeodezi gözlemlerindeki hakim doğrultu atıma rağmen fay oldukça düşük eğime (53°–73°) sahiptir. Bu durum arazi gözlemleriyle de uyuşmamaktadır. Bu çalışmada 12 Kasım 1999 Düzce depreminin neden olduğu yeryüzü deformasyonu yapay açıklık radar interferometrisi (InSAR) yöntemi ile haritalandı ve kırık geometrisini ortaya çıkarmak için elde edilen bu veriler eşzamanlı GPS verileri ile birlikte modellenildi. Modellenmede elastik yerdeğiştirme yöntemi kullanıldı. Yapılan modellerden muhtemelen Düzce depreminin çok kırıklı bir deprem olabileceği ve düşey konumlu Düzce Fayı ile birlikte kuzeye doğru eğimli eski bir bindirme düzleminin de kırılmış olabileceği ihtimali ortaya çıkmaktadır.

Anahtar Sözcükler: Düzce depremi, SAR interferometrisi, GPS, elastik modelleme, deprem kaynak parametreleri

Introduction

The Düzce area was struck once more by a large earthquake on 12 November 1999, 87 days after the devastating 17 August 1999 İzmit (Mw=7.4) earthquake that occurred to the west in the Sea of Marmara region (Figure 1) (Barka *et al.* 2002). The two adjoining earthquakes produced a surface rupture about 200 km long along the North Anatolian Fault Zone (NAFZ). The Düzce earthquake (Mw=7.2) is the latest strong

earthquake in a sequence of westward migrating earthquakes since the 1939 great Erzincan earthquake (Mw=8.0). This sequence has been interpreted as being triggered due to Coulomb stress transfer (Stein *et al.* 1997; Nalbant *et al.* 1998). In this context, the Düzce earthquake was expected by Barka (1999), who, after the İzmit earthquake, defined the Düzce area as a potential seismic gap taking into account the fact that the Düzce Fault was the only segment of the NAFZ in the region that did not break.

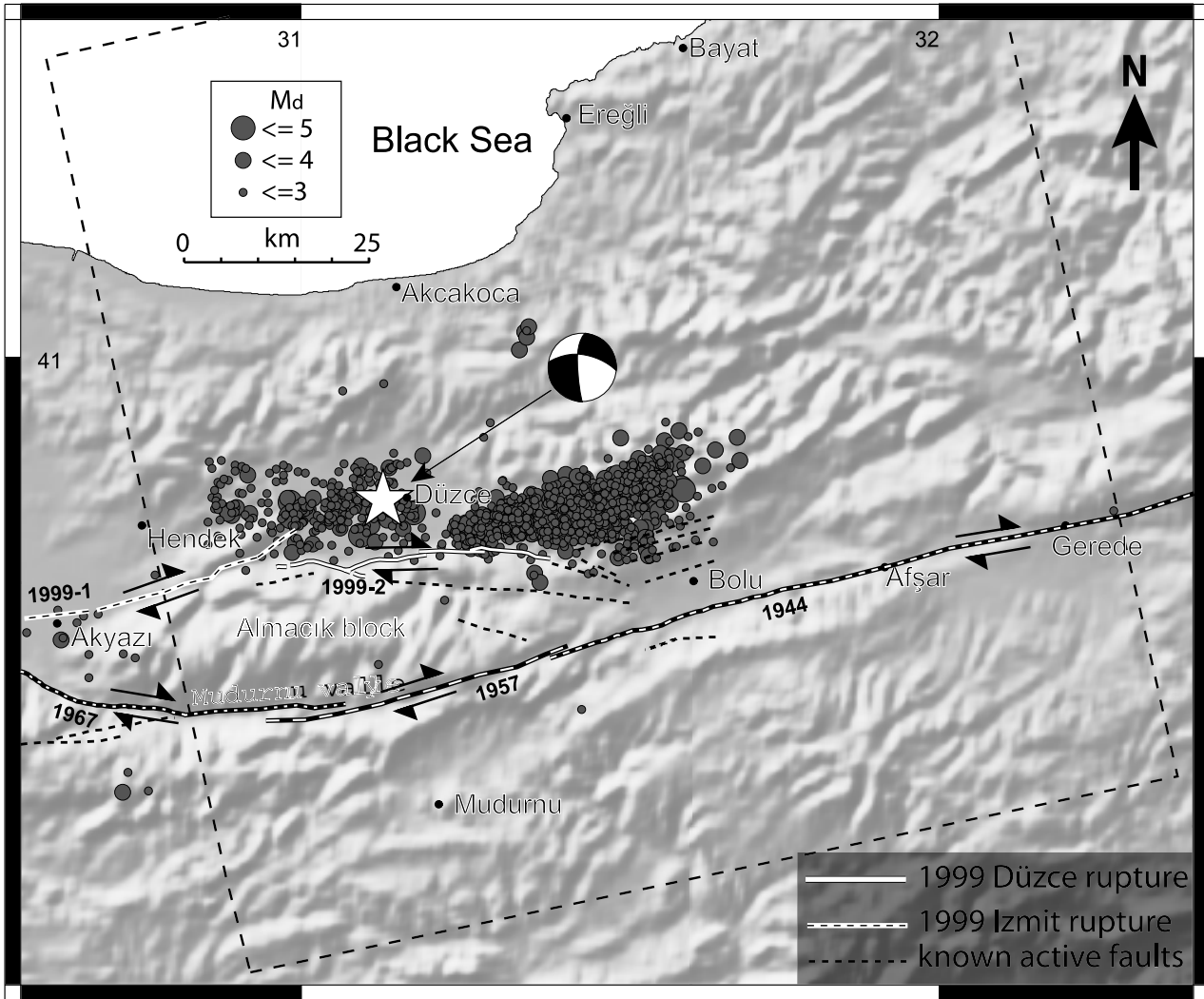


Figure 1. The 1999 and previous earthquake's breaks and neighbouring active faults. The star denotes the epicentre of main shock of the Düzce earthquake with the focal mechanism solution from Harvard CMT, with location from Özalaybey *et al.* (2000). Circles are aftershocks recorded between 12/11/99 and 20/11/99 by the TÜBİTAK permanent network (Özalaybey *et al.* 2000). The background DEM image is from GTOPO30. The dashed box shows the location of the ERS Interferograms (Frame 812, Track 114).

In this study, the coseismic deformation field of the Düzce earthquake is mapped using Synthetic Aperture Radar Interferometry (InSAR), a powerful remote sensing technique for studying surface deformation with high accuracy and spatial sampling (Massonnet *et al.* 1993; Peltzer *et al.* 1996; Massonnet & Feigl 1998; Bürgmann *et al.* 2000). Coseismic interferograms are calculated from ERS SAR images. Using elastic dislocations on rectangular fault planes embedded in a homogeneous half space, we model the SAR observations to deduce the source parameters of the Düzce earthquake. Modelling is performed using an iterative

least-squares inversion technique. In addition to the InSAR data, a set of coseismic GPS data published by Ayhan *et al.* (2001) is also used in modelling.

Source parameters of the Düzce earthquake were first deduced from coseismic GPS measurements by Ayhan *et al.* (2001). Using the same interferogram used here and the GPS measurements of Ayhan *et al.* (2001) with some additional vectors, Bürgmann *et al.* (2002) proposed more detailed models of slip distribution for the Düzce earthquake. These studies state that the Düzce rupture must dip strongly to the north (55° – 59°), an inference that is consistent with seismological observations but

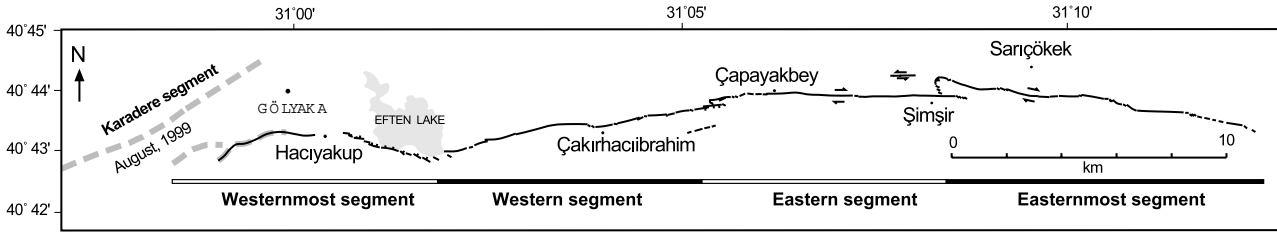


Figure 2. Surface rupture map of the November 12 1999 Düzce earthquake (from Akyüz *et al.* 2002).

contradicts previous geological studies in which a south-dipping Düzce Fault is proposed (Şengör *et al.* 1985; Armijo *et al.* 1999). Both Ayhan *et al.* (2001) and Bürgmann *et al.* (2002) assume a single fault rupture. However, we will demonstrate that the slip models with a multiple-fault-rupture that involves a vertical Düzce Fault can also explain the geodetic data set reasonably well. In the first stage of modelling, we model the geodetic data also with a single fault rupture after finding an overall optimum fault dip found through joint and separate inversions of the observed data set. Then, taking into account the tectonic field observations and well-located aftershocks (Özalaybey *et al.* 2000), the geodetic data set is simulated by inverting subsurface slip on multiple faults.

Tectonic Background and Field Observations of the Fault Rupture

The NAFZ is expressed as a well-defined narrow deformation zone to the east of Bolu, where it splays into two major branches to the west towards the north Aegean (Figure 1). The southern branch runs through Lake Abant and Mudurnu Valley. The Düzce Fault splays from the southern branch of the NAFZ in a complex, 10- to 20-km-wide right stepover. Several intervening short faults are located within the stepover and accommodate the transfer of slip between the northern (i.e. Düzce Fault) and southern branches (Altunel *et al.* 2000; Barka *et al.* 2001). To the west near Gölyaka, there is a sharp change ($> 30^\circ$) in the strike of the northern branch of the NAFZ from E–W to NE–SW. The NE–SW trending portion of the fault is the Karadere segment that ruptured in the 17 August 1999 İzmit event (Hartleb *et al.* 2002). The southern branch was completely broken by the 1944 Bolu-Gerede, 1957 Abant, and 1967 Adapazarı earthquakes. Towards the west, the two branches merge

in a deformation zone between Akyazı and Sapanca, bordering the Almacık block. With the 1999 earthquake sequence this block is now surrounded almost completely by recent fault breaks (Figure 1).

Detailed field observations describing rupture geometry and slip distribution were reported by Akyüz *et al.* (2002). Here, a brief summary relevant to this study is given. The rupture trends E–W in general and it is approximately 40 km in length from Kaynaşlı in the east to Gölyaka in the west.

The abundance of man-made features, such as roads and fences that were offset by the fault rupture, made it possible to measure the displacements very accurately and frequently. The rupture is confined in a generally narrow deformation zone (5–50 m). Considering its geometry and the along-strike slip distribution, the rupture can be divided into four sub-segments (Figure 2). While the three segments in the east show almost pure right-lateral slip up to 5.5 m in the middle one, the westernmost segment experienced an oblique slip with a (down-to-the-north) normal slip component up to 3.5 m. The distribution of the coseismic slip along the rupture is fairly simple with high slip occurring in the centre and tapering off symmetrically towards both edges. Eastern segments are separated by two right stepovers about 1 km wide, within which thrusting and left-lateral displacements arising from block rotations were observed. The westernmost segment can be considered an oblique transfer fault that connects the NE–SW trending Karadere Fault to the E–W-trending Düzce Fault. This change in the fault geometry leads to the formation of a releasing stepover zone, which explains the present-day morphology in the Gölyaka area where the Düzce Basin is bordered by the north-facing, steep fault scarps with triangular facets and the Eften Lake in the immediate hanging-wall. This stepover may have

acted as a geometric barrier to the propagation of the 17 August 1999 İzmit earthquake (cf. Barka & Kadinsky-Cade 1988). After the İzmit earthquake, surface cracks were observed along the westernmost segment, which is interpreted as sympathetic slip on an adjacent fault (Hartleb *et al.* 2002). Focal mechanism solutions of the Düzce earthquake indicate that the fault dips to the north at an angle ranging from 53° to 73° with a rake between 167° and 184° (Table 1). The fact that the majority of the aftershocks are located on the northern side of the fault and that the earthquake epicentre is located in the alluvial plain about 5–8 km north of the surface rupture also confirms the inference that the fault has a significant northward dip. In contrast to the seismological observations, except along the westernmost segment, no indication of such a low-angle fault dip or significant rake was observed in the field. The north-dipping fault geometry also contradicts previous studies (Şengör *et al.* 1985; Armijo *et al.* 1999), in which a south-dipping transpressional fault is inferred. In the light of new results found in this study these contradictory views on the geometry of the Düzce Fault (Şengör *et al.* 1985; Ayhan *et al.* 2001; Bürgmann *et al.* 2002) will be discussed below.

InSAR Data

The term interferometry is derived from the word interference. Interference is a phenomenon that occurs when one has waves of any kind, such as sound, light, ocean, electromagnetic and seismic. Interference occurs whenever two waves come together. InSAR is a method in which the phenomenon of interference is combined with synthetic aperture radar. A radar interferometer can be formed by relating the signals from two spatially

separated radar antennas. The two antennas may be mounted on a single platform (for aircraft usually) (single pass interferometry), or a synthetic interferometer may be realised by utilising a single antenna on a satellite in a nearly exact repeating orbit, in which case the baseline is formed by relating radar signals on repeat pass over the same scene (repeat passes interferometry). A radar image contains both the amplitude and the phase of the electromagnetic signals reflected from targets within the imaging area. InSAR uses the phase information in two SAR images by calculating the phase difference between each pair of corresponding image points after precisely aligned to a fraction of a pixel width. The resulting new image is called an interferogram. The interferogram is an interference pattern of fringes due to relative phase difference, effectively a contour map of the change in the distance from the radar to the ground surface. Each cycle of phase, or fringe, in the resulting interferogram corresponds to a change in range distance from the satellite or aircraft to the ground surface equal to one-half of the radar wavelength ($5.66/2 = 2.83$ cm for ERS). Relative phase difference occurs as a result of slightly different viewing angles (hence the topography), changes on the Earth's surface, and tropospheric delays in the radar signal. Therefore, when the phase difference due to the different viewing geometry (i.e. topographic phase) is removed from the interferogram, the remaining phase difference will practically show surface change only, assuming that no atmospheric artifacts exists. To measure the movements of the Earth's surface by InSAR, therefore, two images of an area taken at different times are required. When the necessary conditions, such as good orbital separation and same target reflectivity, are met the surface movements that occur in the time interval between the two data acquisitions will be captured by

Table 1. Parameters of the 1999 Düzce earthquake compiled from the following sources: UGGS– USA Geological Survey, HVD– Harvard University, CSEM– European-Mediterranean Seismological Centre, OBN– Obninsk Seismological Observatory, Obninsk, Russia, GFZ– GeoForschungsZentrum Potsdam (Bock *et al.* 2000), ERD– Earthquake Research Department (Disaster Affairs, Ankara), TUBI: TÜBİTAK-Marmara Research Centre (Özalaybey, pers. comm. 2002).

Source	E (°)	N (°)	Depth (km)	Mw	Strike (°N)	Dip (°)	Rake (°)	Mo (Nm)
USGS	31.161	40.758	19.0	7.1	269	73	177	5.6 10 ¹⁹
HVD	31.250	40.930	18.0	7.2	268	54	167	6.7 10 ¹⁹
CSEM	31.161	40.758	15.0	7.0	282	74	170	4.1 10 ¹⁹
OBN	40.758	31.161	15.0	7.3	260	53	175	9.1 10 ¹⁹
ERD	31.21	40.79	11.0	7.2	–	–	–	–
GFZ	–	–	–	7.1	264	64	184	4.6 10 ¹⁹
TUBI	31.16	40.83	9.6	–	–	55	–	–

InSAR very accurately (sub-centimetre) with a fine resolution and high spatial distribution (100 x 100 km for ERS satellites). The movements on the Earth's surface can be due to earthquakes, plate movements, volcanoes, glaciers, landslides, salt diapirism, groundwater and petroleum extraction and land watering. What is measured by radar is not the absolute range change, but only the relative phase change between 0 and 2π (one wavelength). Thus, two targets will appear at the same phase if their ranges differ by an integral number of wavelengths. It is therefore necessary to find the multiples of 2π that disappeared or wrapped. Unwrapping can be performed manually by digitising the fringes and multiplying by 2π (contour line unwrapping) (Wright *et al.* 1999), or automatically by using unwrapping algorithms (regional 2D unwrapping) (Gens & Vangenderen 1996).

Three ERS SAR images were requested and processed, one about a month before the earthquake and one tandem pair ten days after. The images were acquired at the ascending pass of the satellite (Figure 1). Two coseismic interferograms were calculated using the ROI-PAC software package developed jointly by the Jet Propulsion Laboratory of NASA and the California Institute of Technology (Rosen *et al.* 1996). To increase the coherence, the interferograms are processed at 2 by 10 looks, resulting in a pixel size of 40 x 40 m (20 x 2–4 x 10). A 30-second posting DEM (USGS GTOPO30) is simulated to remove the topographic contribution from the interferograms. One of the interferograms (not shown here) has a very low coherence (pair 2, see Table 2). This can be attributed to the small altitude of ambiguity h_a of the pair (37 m in the scene centre). The altitude of ambiguity is the elevation difference between two neighbouring topographic fringes in an interferogram and depends on the separation between two orbits. Therefore, if the digital elevation model used to remove to topographic contribution to the interferogram has errors, fringes of topographic residuals will remain in the interferogram. The altitude of ambiguity of the second interferogram is relatively

higher, about 165 m in the centre of the scene, and thus coherence is better than that in the first interferogram (Figure 3). Nevertheless, artifacts resulting from errors in the DEM appear as high frequency short-wavelength signals in the areas with ragged topography, particularly southeast of the fault rupture (Figure 3).

The coseismic interferogram is shown in Figure 3 with wrapped fringes, each representing half a wavelength (i.e. 2.83 cm) range change along the radar line of sight. If we assume that all the displacement is pure right-lateral slip then each fringe represents 7.24 cm of horizontal displacement. Coherency is completely lost in the flat Düzce plain probably owing to a combination of high gradient deformation close to the rupture, and changes in water content and in vegetation cover due to high agricultural activity. It is also generally inadequate in regions of ragged topography, particularly around the Almacık block in the south and in the northeast of the fault rupture. Coherence is preserved mainly in the southern parts of the interferogram, but the concave fringes in the north–northwest of the surface rupture can still be seen. In the south, seven continuous fringes representing 19.81 cm of range change along the radar line of sight can be counted, whereas in the north there are at least 15 fringes. The surface rupture trends roughly E–W, sub parallel to the radar look direction (black arrow in Figure 3). Therefore, a dominant strike-slip movement on a steep, near-vertical fault is expected to produce fringes that are nearly symmetrical about the fault rupture, which is also because the radar-look direction is roughly parallel to the trend of the rupture. However, this is not the case; while the fringes in the south trend mainly E–W with low gradient, those in the north have a circular shape with high gradient. This apparent asymmetry confirms the seismological observations that suggest that the fault dips to the north and the displacement is not pure dextral-slip.

Because the interferogram spans a period of ten days after the Düzce earthquake, it may also contain some transient postseismic deformation as observed in the

Table 2. Details of the image pairs used for constructing coseismic interferograms and their corresponding values of altitude of ambiguity (h_a). B– represents the perpendicular baseline component of orbital separation.

Pair	Track	Frame	Orbit1	Date-1	Orbit2	Date-2	B– (m)	h_a (m)	T. Baseline (day)
1	114	812	23014	14 September 1999	43689	22 November 1999	67	165	69
2	114	812	23014	14 September 1999	24016	23 November 1999	258	37	70

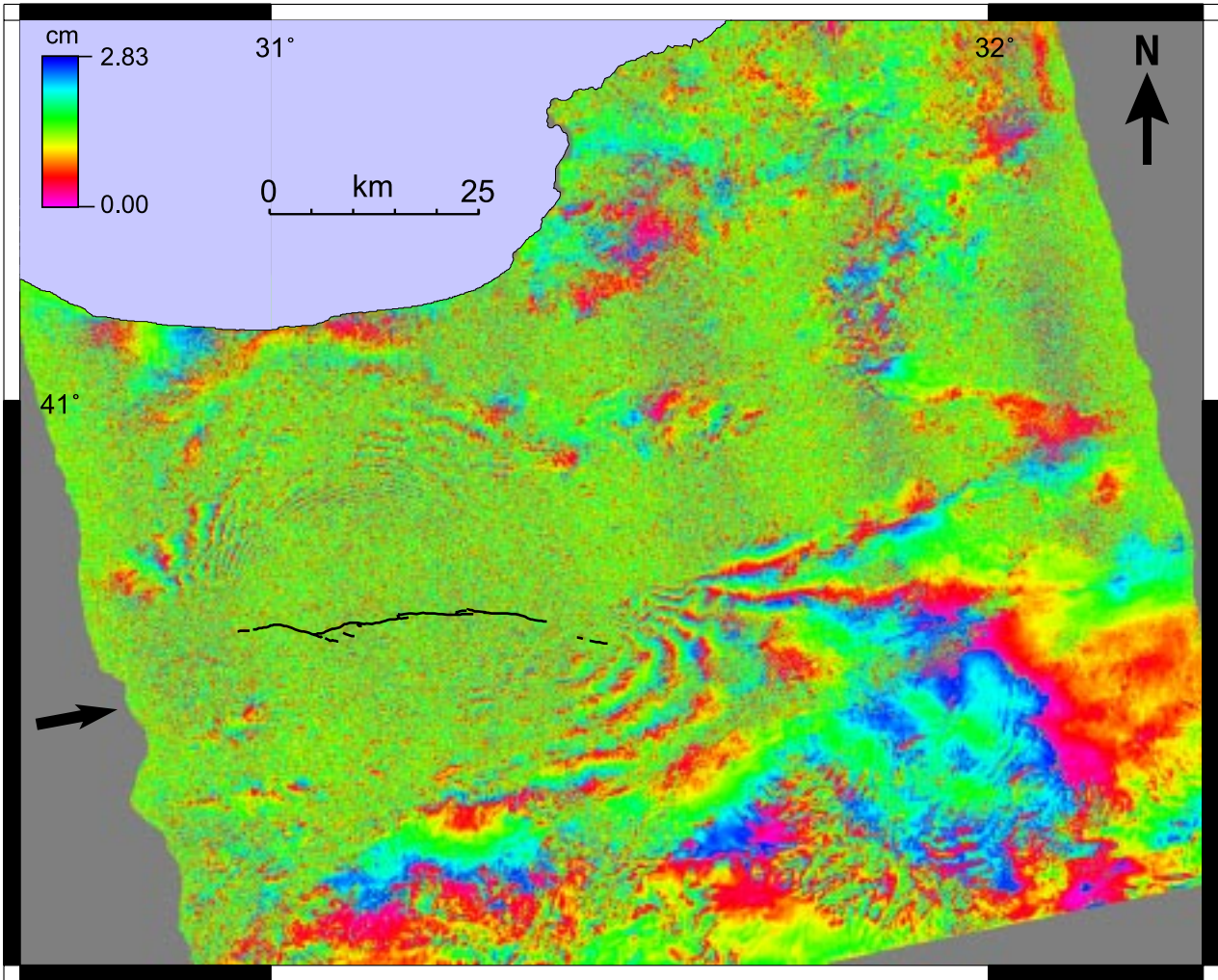


Figure 3. Coseismic interferogram of the 12 November 1999 Düzce earthquake. Each fringe represents 2.83 cm of range change along the radar line of sight. Surface rupture is shown with black lines. The radar-look direction is indicated by a black arrow.

İzmit coseismic interferograms (Çakır *et al.* 2003). In order to avoid misinterpretations of the data, the possible presence of atmospheric artifacts in the interferogram is also checked using the technique described by Çakır *et al.* (2002), and it is found that atmospheric contamination in the interferogram is not significant enough to be modelled and removed.

Modelling with Elastic Dislocations

Because of its low coherence, the interferogram was not unwrapped. Instead, the visible fringes in the interferogram were digitised and sampled. The sampled SAR data (1315 measurements) and three components of the coseismic GPS measurements (52 x 3 sample) are

modelled using rectangular dislocations in an elastic, homogeneous and isotropic half-space (Okada 1985).

Fault geometry plays a key role in determining the subsurface slip when modelling geodetic data with elastic dislocations. The better the fault geometry is constrained the more accurate the solution that is found through inversions and forward modelling. Tectonic field observations thus provide an essential piece of information and reduce considerably the range of possible solutions. The inversions can allow one to estimate simple fault geometry only. Complicated fault ruptures such as those involving multiple faults with varying dip and strike are difficult to estimate without additional information such as tectonic field observations and seismicity.

The preliminary modelling of the geodetic data set indicates that the rupture must dip to the north, in agreement with seismological observations (Table 1) and previous studies (Ayhan *et al.* 2001; Bürgmann *et al.* 2002). Therefore, an optimum fault dip required by the InSAR and GPS data is sought by inverting them separately and jointly using an inversion algorithm based on a least-squares approximation. The model fault used in the inversions is 18 km wide and 48 km long. The fault length is kept longer than it is observed in the field so that the eastern extent of the coseismic slip can be resolved. Preliminary modelling also indicates that a longer fault is also required by the two geodetic data sets. The model fault trends nearly in the E–W (N88°E) direction and roughly coincides with the mapped surface rupture at the surface. The fault is divided into 12 patches of 4 km long along the strike so that the modelled slip can vary along the strike. Keeping all the parameters fixed the geodetic data set is inverted for uniform slip on each patch with dips varying from 30° to 90° (Figure 4). As shown in Figure 4, the GPS data require a steeper dip angle (54°) than the InSAR data (67°). If the two data sets are jointly inverted weighting them equally, the optimum dip angle for the two data sets is found to be 62°. An overall optimum rake is also sought using the same approach and is found to be 10°. This range of dip angle and the rake are consistent with independent seismological evidence (Table 1).

In order to obtain a slip model that varies also at depth, the fault is further discretised into 4.5-km-wide patches along the dip (48 patches in total). The uniform slip model with a dip of 62° is used as a starting solution in all the inversions. The uppermost patches are, however, constrained by the field observations because the resolution of the InSAR and GPS data is relatively lower in the near field. Because the starting model explains most of the InSAR and GPS data very well (rms=2.1 cm), the inversions are stable and give similar solutions (Figure 5). While all the models fit fairly well to the InSAR data in the northern side of the fault, the fit in the south is not very good (Figure 6a). This poor fit can be attributed to atmospheric artifacts and the simple geometry of the model fault. Nevertheless, the overall fit is within the uncertainty level of the geodetic data since the models explain the InSAR data with an rms error of around half a fringe (1.4 cm). Good fit between the models and the observations is illustrated with some

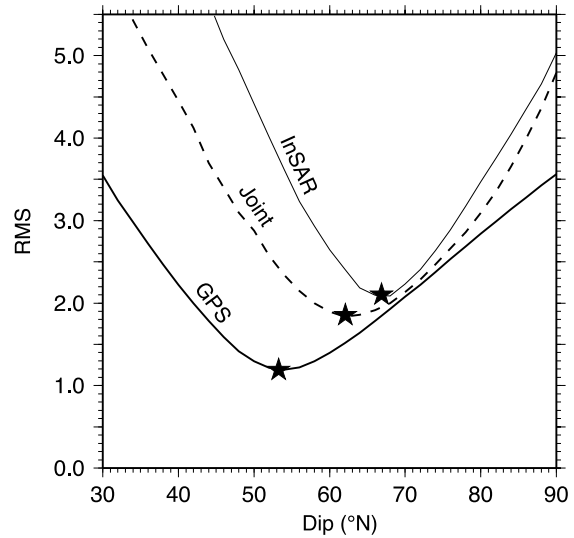


Figure 4. Plots of RMS (root mean square) versus fault dip for the Düzce rupture derived from separate and joint inversion of the geodetic data set using a uniform slip model along depth. The GPS data requires less, about 14°–15°, fault dip than do the InSAR data. Optimal dip for the joint data set is about 62°. Model with a 62° – north-dipping fault geometry is used as starting solution for the variable slip inversions (see text for more information).

selected profiles of range change in Figure 6b. Some discrepancies between the GPS observation and the GPS model are apparent, most likely due to the complexities in the rupture geometry and the slip distribution that are missing in the model parameterisation. Figure 5 shows the strike-slip distributions inverted from the InSAR data, the GPS data, and the joint data set. The overall pattern of slip distribution in all the models is very similar. Both the GPS and InSAR data suggest a similar shape and similar amount of slip, and hence the same geodetic moments. The slip distribution predicted by the two data sets for the Düzce Fault is fairly simple, with coseismic slip reaching a maximum around the fault centre and gradually diminishing towards the edges and towards the deeper parts of the fault rupture. The highest coseismic slip predicted by the both data sets occurs within the upper 15 km of the seismogenic crust, and it reaches up to 6.2 m. The GPS model predicts less slip in the west but more slip in the east compared to the InSAR model. The slip distribution obtained by the joint inversion simply lies in between the two models found from the separate inversions. The geodetic moment (equal to coseismic slip \times rupture area \times shear modulus) derived from the models is 6.1×10^{19} Nm (equivalent to $M_w=7.2$) and is

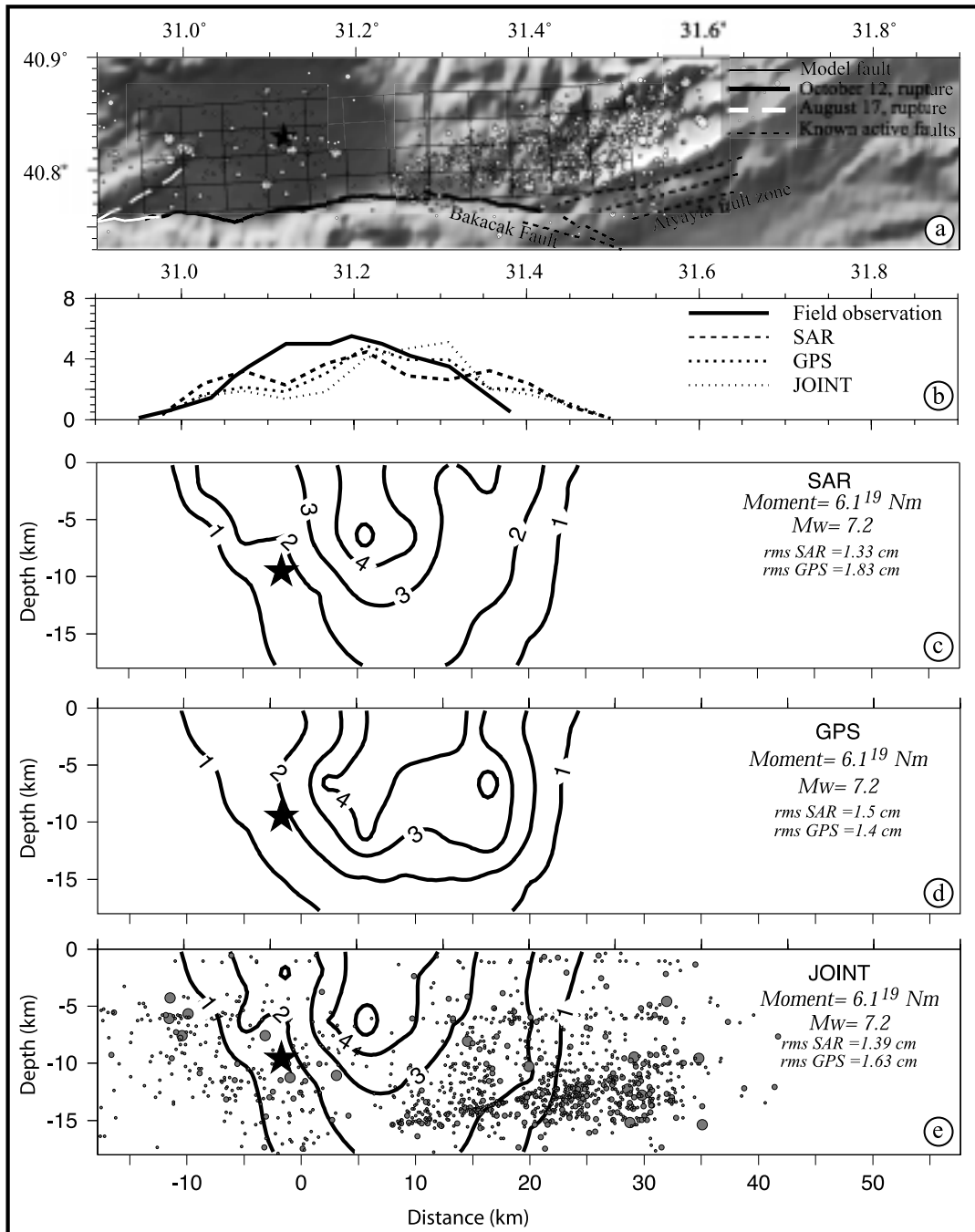


Figure 5. The Düzce earthquake fault trace, the coseismic surface slip and the modelled slip distribution at depth with single-fault-rupture geometry. (a) Shaded topographic map with simplified fault trace and the model fault (rectangles) projected onto the surface. The model fault has 48 patches (4 km x 4.5 km) and dips 62° to the north. Location of the main shock (star) and of aftershocks (white circles) as in Figure 1. (b) Surface right-lateral slip observed and predicted by SAR, GPS and joint inversions. (c) The InSAR model with a view from south to north. Star represents the hypocentre of the main shock with the aftershocks shown with grey circles. (d) The GPS model (data from Ayhan *et al.* 2001). (e) The slip distribution derived from joint inversion of InSAR and GPS data. Scalar moment (Mo) Magnitude (Mw) and RMS to the ERS and GPS data are indicated for each model.

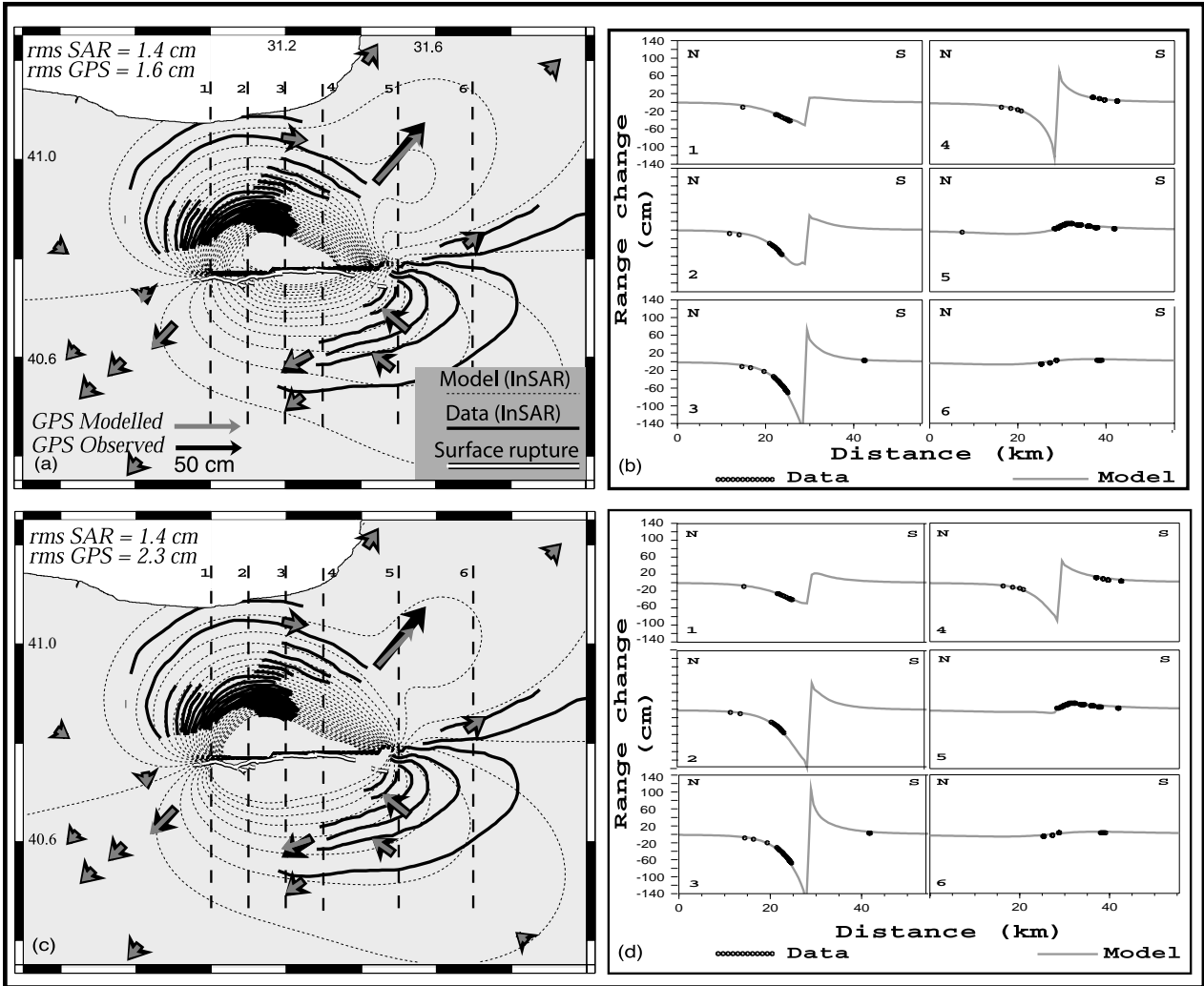


Figure 6. Comparison of the observed data and models. Joint inversion (InSAR and GPS) models with single (a) and multiple (c) fault-rupture geometry. Model fringes (thin dashed grey lines) are contoured at every 2.83 cm to facilitate comparison with the observed fringes (thick black lines). Black and grey arrows show horizontal component of coseismic GPS vectors and modelled vectors, respectively. Profiles of observed and modelled range changes across the fault along the lines shown in (b) and (d).

comparable with seismological estimations that range between 4.1×10^{19} and 9.1×10^{19} Nm (Table 1).

It is clear from seismic and geodetic observations that at least some portion of the fault rupture must dip to the north at some depth. As stated earlier, the westernmost segment shows such a dip. However, models with faults dipping only along the westernmost segment do not satisfactorily explain the geodetic data. Therefore, a longer fault with a northward dip is required. Westward propagation of the NAFZ is known to have been guided by older deformation zones (Şengör & Yılmaz 1981;

Sengör *et al.* 1985; Elmas & Yiğitbaş 2001). In other words, the present-day trace of the NAFZ coincides with the pre-existing zones of weakness. According to Elmas & Yiğitbaş (2001), the NAFZ (including the Düzce segment), in northwestern Turkey, forms the contact between two distinct tectonic units: the Sakarya block and the western Pontide block. This zone is thought to have accommodated the subduction of the Sakarya Continent underneath the Pontides during the Mid-Jurassic time, and left-ateral motion between the two tectonic units later in the Late Cretaceous time (Elmas & Yiğitbaş 2001). Therefore, it is plausible that the Düzce

Fault is in fact vertical, but cuts an old north-dipping structure at depth that might be an old thrust. In such a case, the Düzce earthquake might have been nucleated on a pre-existent, north-dipping fault plane and propagated upwards rupturing the upper portion of the vertical Düzce Fault.

To test this hypothesis, rupture models consisting of two intersecting faults with an intersection depth varying from 4 to 9 km depth are constructed, and to what extent such models can explain the geodetic data is explored using the inversion procedure described above. The fault that coincides with the surface rupture is always kept vertical and the other is allowed to dip to the north at an angle ranging from 60° to 45° . It is unlikely that the two faults strike parallel to each other. However, because construction of a rupture geometry using rectangular patches of different strike and dip results in gaps and overlaps between the rectangular faults, the two faults are assumed to be parallel. The tests performed show that the geodetic data can be well explained with multiple-fault models with an intersection depth down to 8 km, and that the minimum depth for a fault intersection that can be resolved is about 4 km. A rupture model with an intersection depth of 8 km is shown in Figure 7 with the inverted slip on it. The geodetic observations are in good agreement with the

synthetic data derived from this model (Figure 6c). The model predicts the InSAR data with the same RMS error of 1.4 cm as does the previous model with the single-fault-rupture geometry. Although the overall match between the observed and modelled GPS vectors is fairly reasonable, the fit is poorer than the one with single-fault-rupture model (rms=2.3 cm) (Figures 6a & c). This is mainly due to the poor fit obtained for the GPS vector northeast of the rupture that might have some measurements errors (Ergintav, pers. comm. 2001). Although the predicted slip distributions are roughly similar to those obtained from single-fault-rupture geometry inversions, some important differences are present. Both the single-fault-rupture models (MOD-1) and the multiple-fault-rupture models (MOD-2) suggest a similar pattern of slip distribution along the western half of the fault. However, to the east the coseismic slip deduced from the MOD-2 type model is less than that deduced from the MOD-1 type model. The magnitude of slip in the MOD-2 type model is much higher on the deeper parts of the rupture. The overall amount of slip and thus geodetic moment is slightly higher 3–5(%) in the MOD-2 type model (Figure 7). Although the overall fit of the MOD-2 type model to the geodetic measurements is reasonable, some discrepancies remain. Inadequate fit can be attributed to simple parameterisation of the fault

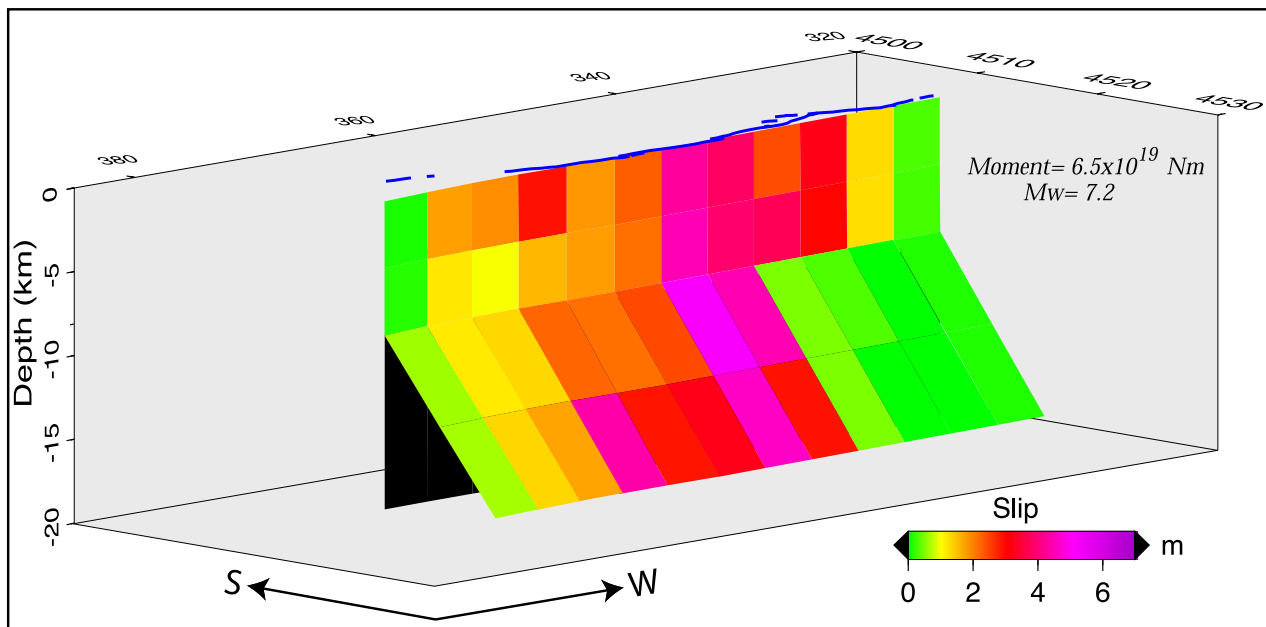


Figure 7. A 3D perspective view of the slip distribution deduced from joint inversion using multiple-fault-rupture geometry.

rupture, simplifying assumptions in the calculations of surface deformation (homogeneous crust, no topography, elastic properties of rocks, etc.). For example, the strike of the model fault is rather inconsistent with the strike of the easternmost segment of the surface rupture. A good fit could not be obtained with model faults trending parallel to the strike of the easternmost segment, suggesting that the rupture probably also bifurcates to the east, and thus the composite nature of the rupture is more complicated than is assumed in the models.

Most of the aftershocks northeast of the rupture appear to be associated with thrust faulting (Özalaybey, pers. comm. 2002), suggesting that the Atyaylası fault zone (Figure 5a) dips to the north and has a significant reverse component. This inference is also supported by interseismic GPS observations that suggest compression in this region (Straub *et al.* 1997). To illustrate the location and geometry of the model faults with respect to the distribution of the aftershock at depth, some N-S profiles roughly perpendicular to the fault rupture are shown in Figure 8b. The deformation associated with the earthquakes that occur on dipping faults is typically concentrated on the hanging-wall block. Therefore, because the aftershocks are mostly located below the fault used in the MOD-1 type model, the MOD-2 type model seems to be more compatible with the distribution of the aftershocks.

Results and Discussion

The available geodetic data set can be explained by the models with either single- or multiple-fault-rupture geometry within the uncertainty level of the geodetic data set. Inadequate coherence of the InSAR data and lack of GPS points particularly in the near field allow models with both types of rupture geometry to fit the geodetic data within the acceptable limit of error. Therefore, a better spatial coverage of geodetic observations is required for a better constrain on the fault geometry. Nevertheless, the MOD-2 type model is preferred taking into account the fact that the Düzce rupture with a predominant strike-slip trends parallel to the strike of the almost pure strike-slip, vertical fault rupture of the İzmit earthquake to the west, and that the Düzce Fault forms part of a major strike-slip plate boundary between the Anatolian Block and the Eurasian Plate. Accommodating a

significant horizontal motion in the long term via a fault with such a significant fault dip (as in the MOD-1 type model) is mechanically difficult to explain. To some extent, this inference is also consistent with that of Şengör *et al.* (1985), in which a near-vertical south-dipping Düzce Fault is suggested. Bürgmann *et al.* (2002) inverted the same InSAR and GPS data jointly for subsurface slip using single-fault-rupture geometry with 54° north dip and found a slip distribution similar to that found by Ayhan *et al.* (2001), who made use of GPS data only. Their fault geometry and the distribution and magnitude of slip are also in good agreement with the MOD-1 type model found in this study. As they used single-fault-rupture geometry only, they have concluded that the geodetic data rule out the possibility of the Düzce Fault having near-vertical geometry. However, as illustrated above, a composite fault rupture encompassing a vertical Düzce Fault can also explain the geodetic observations reasonably well.

All the models indicate that the two geodetic data sets are generally consistent with each other. This observation in turn suggests that the contribution of the postseismic deformation (about ten days) to the InSAR data is insignificant following the earthquake. Therefore, in contrast to the 17 August 1999 İzmit event (Çakır *et al.* 2003), a fast dynamic after-slip does not seem to have occurred following the Düzce earthquake. The differences between the GPS- and InSAR-derived solutions can be ascribed to different spatial coverage of the two data sets, possible orbital and atmospheric artifacts in the InSAR data and unrecognised errors in the GPS data. Both the GPS and InSAR data suggest a longer (~15 km) fault rupture to the east than the one mapped in the field. This explains why the magnitude of the Düzce event is surprisingly high considering its short rupture length observed in the field. Another factor that leads to the high moment release is that the fault rupture area is larger since the rupture is not entirely vertical.

Acknowledgements

SAR data are provided by ESA under contract A03-354. Financial support from CNRS and TÜBİTAK is gratefully acknowledged.

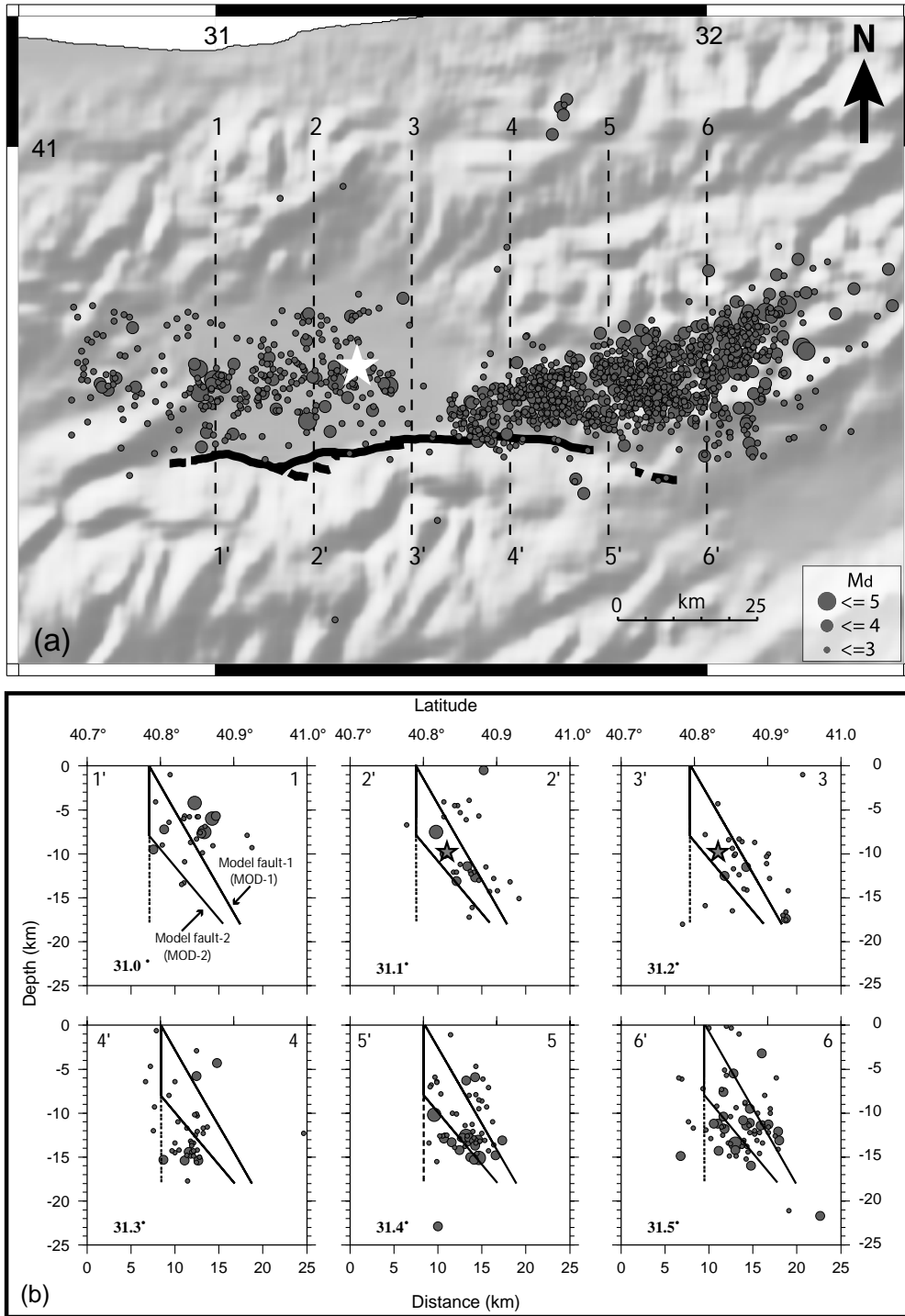


Figure 8. Distribution of aftershocks. (a) Aftershocks recorded between 12/11/99 and 20/11/99 by the TÜBİTAK Marmara Research Centre (Özalaybey *et al.* 2000). Thick black lines show the surface rupture of the 1999 Düzce event. The white star denotes the epicentre of the Düzce main shock (b) Cross-sections showing the aftershock distribution at depth with respect to the two different fault geometries used in the inversions. Locations are shown with a dashed line in (a).

References

- ALTUNEL, E., BARKA, A.A., ÇAKIR, Z., KOZACI, Ö., HITCHCOCK, C., HELMS, J., BACHHUBER, J. & LETTIS, W. 2000. What goes on at the eastern termination of the November 12, 1999 Düzce earthquake, M=7.2, North Anatolian Fault, Turkey. *American Geophysical Fall Meeting, California, USA, Abstracts*, p. F816.
- AKYÜZ, H.S., HARTLEB, R., BARKA, A.A., ALTUNEL, E., SUNAL, G., MEYER, B. & ARMIJO, R. 2002. Surface rupture and slip distribution of the 12 November 1999 Düzce earthquake (M 7.1), North Anatolian Fault, Bolu, Turkey. *Bulletin of the Seismological Society of America* **92**, 61–66.
- ARMİJO, R., MEYER, B., HUBERT, A. & BARKA, A.A. 1999. Westward propagation of the North Anatolian Fault into the northern Aegean: Timing and kinematics. *Geology* **27**, 267–270.
- AYHAN, M.E., BÜRGMANN, R., McCLUSKY, S., LENK, O., AKTUĞ, B., HERECE, E. & REILINGER, R.E. 2001. Kinematics of the Mw=7.2, 12 November 1999, Düzce, Turkey earthquake. *Geophysical Research Letters* **28**, 367–370.
- BARKA, A.A. 1999. The 17 August 1999 İzmit earthquake. *Science* **285**, 1858–1859.
- BARKA, A.A. & KADINSKY-CADE, K. 1988. Strike-slip fault geometry in Turkey and its influence on earthquake activity. *Tectonics* **7**, 663–684.
- BARKA, A.A., ALTUNEL, E., AKYÜZ, S., ÇAKIR, Z., KOZACI, O., LETTIS, W., BACHHUBER, J., HITCHCOCK, C. & HELMS, J. 2001. Seismic Activity and Fault Segmentation of the NAF in the Bolu Mountain: Relationship between the November 12, 1999 and the February 1, 1944 Earthquakes. *EUG XI Meeting, Abstracts, Strasbourg, France*, p. 295.
- BARKA, A.A., AKYÜZ, S.H., ALTUNEL, E., SUNAL, G., ÇAKIR, Z., DIKBAŞ, A., YERLİ, B., ARMIJO, R., MEYER, B., DE CHABALIER, J.B., ROCKWELL, T., DOLAN, J.R., HARTLEB, R., DAWSON, T., CHRISTOFFERSON, S., TUCKER, A., FUMAL, T., LANGRIDGE, R., STENNER, H., LETTIS, W., BACHHUBER, J. & PAGE, W. 2002. The surface rupture and slip distribution of the 17 August 1999 İzmit earthquake M=7.4, North Anatolian Fault. *Bulletin of the Seismological Society of America* **92**, 43–60.
- BOCK, G., TİBİ, R., BAUMBACH, M., GROSSER, H., MILKEREIT, C., KIND, R. & ZSCHAU, J. 2000. Rupture processes of the August 17 İzmit and November 12, 1999 Düzce earthquakes. In: BARKA, A.A., KOZACI, O., AKYÜZ, S. & ALTUNEL, E. (eds), *The 1999 İzmit and Düzce Earthquakes: Preliminary Results*. İstanbul Technical University Publication, 105–108.
- BÜRGMANN, R., ROSEN, P.A. & FIELDING, E.J. 2000. Synthetic aperture radar interferometry to measure Earth's surface topography and its deformation. *Annual Review in Earth and Planetary Sciences* **28**, 169–209.
- BÜRGMANN, R., AYHAN, M.A., FIELDING, E.J., WRIGHT, T., McCLUSKY, S., AKTUĞ, B., DEMİR, C., LENK, O. & TÜRKEZER, A. 2002. Deformation during the 12 November 1999, Düzce, Turkey Earthquake, from GPS and InSAR Data. *Bulletin of the Seismological Society of America* **92**, 161–171.
- ÇAKIR, Z., DE CHABALIER, J.B., ARMIJO, R., MEYER, B., BARKA, A.A. & PELTZER, G. 2003. Coseismic and early postseismic slip associated with the 1999 İzmit earthquake (Turkey), from SAR interferometry and tectonic field observations. *Geophysical Journal International* (in press).
- ÇAKIR, Z., DE CHABALIER, J.B., RIGO, A., ARMIJO, R., BARKA, A. & MEYER, B. 2002. Atmospheric artefacts in SAR interferometry, implications on interpretation and modelling surface deformation: a case study of the 1999 (Mw=7.4) İzmit earthquake, Turkey. *1st International Symposium of the Faculty of Mines (İTÜ) on Earth Sciences and Engineering, 16–18th May 2002, İstanbul, Turkey, Abstracts*, p. 67.
- ELMAS, A. & YİĞİTBAŞ, E. 2001. Ophiolite emplacement by strike-slip tectonics between the Pontide Zone and the Sakarya Zone in northwestern Anatolia, Turkey. *International Journal of Earth Sciences* **90**, 257–269.
- GENS, R. & VANGENDEREN, J.L. 1996. SAR interferometry—issues, techniques, applications. *International Journal of Remote Sensing* **17**, 1803–1835.
- HARTLEB, R.D., DOLAN, J.F., AKYÜZ, H.S., DAWSON, T.E., TUCKER, A.Z., YERLİ, B., ROCKWELL, T.K., TORAMAN, E., ÇAKIR, Z., DIKBAŞ, A. & ALTUNEL, E. 2002. Surface rupture and slip distribution along the Karadere segment of the 17 August 1999 İzmit and the western section of the 12 November 1999 Düzce, Turkey, earthquakes. *Bulletin of the Seismological Society of America* **92**, 67–78.
- MASSONNET, D., ROSSI, M., CARMONA, C., ADRAGNA, F., PELTZER, G., FEIGL, K. & RABAUTE, T. 1993. The displacement field of the Landers earthquake mapped by radar interferometry. *Nature* **364**, 138–142.
- MASSONNET, D. & FEIGL, K.L. 1998. Radar interferometry and its applications to changes in the Earth's surface. *Reviews of Geophysics* **36**, 441–500.
- NALBANT, S.S., HUBERT, A. & KING, G.C.P. 1998. Stress coupling between earthquakes in northwest Turkey and the North Aegean Sea. *Journal of Geophysical Research* **103**, 24469–24486.
- OKADA, Y. 1985. Surface deformation due to shear and tensile faults in a half-space. *Bulletin of the Seismological Society America* **75**, 1135–1154.
- ÖZALAYBEY, S., AKTAR, M., ERGİN, M., KARABULUT, H., BOUCHON, M., TAPIRDAMAZ, C., & YORUK, A. 2000. Aftershock Studies Following Recent Earthquakes in Turkey. *XXVII General Assembly of the European Seismological Commission (ESC), Lisbon University, Lisbon, Portugal, September 10–15*, p. 31.
- PELTZER, G., ROSEN, P., ROGEZ, P. & HUDNUT, K. 1996. Postseismic rebound in fault step-overs caused by pore fluid flow. *Science* **273**, 1202–1204.
- ROSEN, P., HENSLEY, S., ZEBKER, H., WEBB, F.H. & FIELDING, E.J. 1996. Surface deformation and coherence measurements of Kilauea volcano, Hawaii, from SIR-C radar interferometry. *Journal of Geophysical Research* **101**, 23109–23125.

- ŞENGÖR, A.M.C. & YILMAZ, Y. 1981. Tethyan evolution of Turkey: A plate tectonic approach. *Tectonophysics* **75**, 181–241.
- ŞENGÖR, A.M.C., GÖRÜR N. & ŞAROĞLU, F. 1985. Strike-slip faulting and related basin formation in zones of tectonic escape: Turkey as a case study. In: BIDDLE, K. T. & CHRISTIE-BLICK, N. (eds), *Strike-slip Faulting and Basin Formation*. Society of Economic Paleontologists and Mineralogists Special Publications **37**, 227–264.
- STEIN, R.S., BARKA, A.A. & DIETERICH, J.H. 1997. Progressive failure on the North Anatolian Fault since 1939 by earthquake stress triggering. *Geophysical Journal International* **128**, 594–604.
- STRAUB, C., KAHLE, H.G. & SCHINDLER, C. 1997. GPS and geologic estimates of the tectonic activity in the Marmara region, NW Anatolia. *Journal of Geophysical Research* **102**, 27587–27601.
- WRIGHT, T.J., PARSONS, B.E., JACKSON, J.A., HAYNES, M., FIELDING, E.J., ENGLAND, P.C. & CLARKE, P.J. 1999. Source parameters of the 1 October 1995 Dinar (Turkey) earthquake from SAR interferometry and seismic body wave modeling. *Earth and Planetary Science Letters* **172**, 23–37.

Received 06 August 2002; revised typescript accepted 05 February 2003